In situ mechanical characterization of mouse oocytes using a cell holding device

Xinyu Liu,†[a] Roxanne Fernandes,[b] Andrea Jurisicova,[b] Robert F. Casper[b] and Yu Sun*[ac]

Received 29th March 2010, Accepted 7th May 2010
DOI: 10.1039/c004706f

This paper presents a cellular force measurement technique that allows for mechanical characterization of mouse oocytes during microinjection (*i.e.*, *in situ*) without requiring a separate characterization process. The technique employs an elastic cell holding device and a sub-pixel computer vision tracking algorithm to resolve cellular forces in real time with a nanonewton force measurement resolution (2 nN at 30 Hz). Mechanical properties (*i.e.*, stiffness) of both healthy and defective mouse oocytes are characterized. The experimental results suggest that the *in situ* obtained force-deformation data are useful for distinguishing healthy mouse oocytes from those with aging-induced cellular defects, promising an approach for oocyte quality assessment during microinjection. Biomembrane and cytoskeleton structures of the healthy and defective oocytes are also investigated in an attempt to correlate the measured subtle mechanical difference to cellular structure changes.

Introduction

Many cellular functions, such as cell division, gene expression, signal transduction, and apoptosis, depend on mediation and regulation of mechanical signals (*i.e.*, forces and stresses), and on mechanical properties of cell membranes and intracellular structures.[1–3] Quantification of cell mechanical properties is not only important for understanding cellular structure and function but also useful for assessing cell quality.[2,4,5] For instance, a range of human diseases are closely correlated with variations of the mechanical properties of cells,[4,5] suggesting cellular mechanical characterization a possible candidate for disease state detection.

For mechanical characterization of a living cell, the cell must be deformed in some way and the applied forces/stresses and cell deformations measured. Experimental techniques for cellular force measurement include micropipette aspiration,[6,7] optical tweezers,[8] optical stretchers,[9] atomic force microscopy (AFM),[10] magnetic bead measurement,[11] and microelectromechanical systems (MEMS) transducer based measurement.[12,13] Among these techniques, MEMS force transducers have certain advantages over other tools due to their cost-effectiveness and flexibility for system integration. However, the construction of MEMS force sensors is typically based on silicon micromachining that requires much processing effort.[12] Furthermore, issues such as biocompatibility and operation in an aqueous environment for biological cells to survive often pose stringent challenges and intricacies in MEMS design, material selection, and microfabrication.

Instead of using silicon-based MEMS transducers, polymeric materials such as polydimethylsiloxane (PDMS) and polyacrylamide (PAM) have been widely employed as passive deformable force sensors for cellular force measurements, due to their high transparency, low stiffness, and biocompatibility. Although PDMS or PAM flexible substrates have been used for characterizing cellular traction forces by visually tracking local deformations of the substrates,[14,15] the continuous deformation model of the substrates requires complex computation to interpolate measured local discrete deformations into global continuous deformations.

PDMS micro-post structures were also demonstrated as force transducers, enabling measurements of local traction forces generated by adherent cells.[16–18] The devices can be easily constructed using standard soft-lithography.[19] Image processing techniques were used for measuring the PDMS post deflection, and only a simple cantilever mechanical model is required for mapping post deflections into cellular forces.

Such micro-post devices were also modified by integrating magnetic nanowires into individual micro-posts so that external magnetic field induced forces can be applied to the cells.[20] The cellular retraction force response to the applied forces was examined, providing an interesting approach to investigate cellular locomotive behavior under mechanical stimuli. Although the polymeric micro-post devices can both apply mechanical stimuli to adherent cells and simultaneously measure their traction forces, they are not suitable for characterizing mechanical properties of suspended cells such as oocytes/embryos.

Microinjection of foreign materials (*e.g.*, proteins, genetic materials, and sperms) into cells is an established technique in biological experiments, which greatly facilitates biomolecule screening[21] and reproductive research.[22,23] This paper presents a cellular force measurement technique and its application to mechanical characterization of mouse oocytes during

[a]*Department of Mechanical and Industrial Engineering, University of Toronto, 5 King's College Road, Toronto, Ontario, Canada M5S 3G8. E-mail: sun@mie.utornto.ca; Fax: +1-416-978-7753; Tel: +1-416-946-0549*
[b]*Samuel Lunenfeld Research Institute, Toronto Mount Sinai Hospital, 600 University Ave, Toronto, Ontario, Canada M5G 1X5*
[c]*Institute of Biomaterials and Biomedical Engineering, University of Toronto, 164 College Street, Toronto, Ontario, Canada M5G 1X5*
† Current address: Department of Chemistry and Chemical Biology, Harvard University, 12 Oxford Street, Cambridge, MA 02138, USA

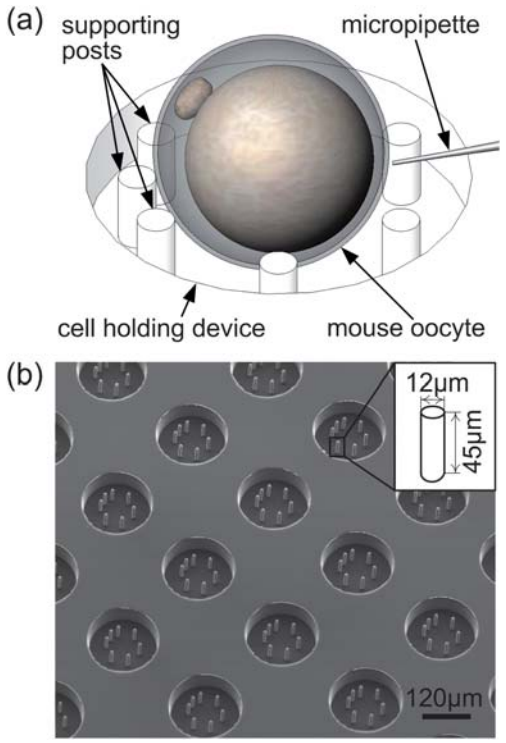

Fig. 1 (a) Schematic of cellular force measurement technique using low-stiffness elastic posts during microinjection. (b) Scanning electron microscopy (SEM) image of a PDMS cell holding device.

microinjection (referred to as *in situ* in this work). A PDMS cell holding device (Fig. 1(a)) and a sub-pixel visual tracking algorithm are used together to visually resolve applied forces to a single oocyte with nanonewton force resolutions.

We previously demonstrated the use of a large-sized PDMS device on zebrafish embryos.[24] The study presented here focuses on miniaturizing the cell holding devices for studying mouse oocytes (90 μm in diameter *vs.* 1.2 mm zebrafish embryos), enhancing the force measurement resolution to the nanonewton level, and attempting to use the *in situ* obtained cell mechanical property information to distinguish healthy mouse oocytes from those with compromised developmental competence. Additionally, new biological results on structural changes of defective oocytes from old mice are presented. Considering the high deformability of mouse oocytes, our present micro-post arrangement employs the minimal number of supporting posts for securely immobilizing an oocyte during microinjection (Fig. 1(a)) and for maximizing post deflections. In addition, the analytical mechanics model ("Force Analysis" Subsection) for calculating the cellular forces was modified based on a new boundary condition.

Stiffness of healthy and defective mouse oocytes were characterized during microinjection. Follow-up structural imaging of the zona pellucida (ZP) and fluorescence analysis of filamentous actin (F-actin) contents verify that structural differences of the ZP and cytoskeleton exist between healthy and defective oocytes. These structural differences are speculated to result from oocyte defects and be responsible for stiffness changes.

Materials and methods

Mouse oocyte preparation

In this study, oocytes from young (8–12 weeks old) and old (40–45 weeks old) imprinting-control-region (ICR) female mice (referred to as young and old oocytes in the rest of this paper) were used. 40–45 weeks old ICR female mice are near the end of their reproductive lifespan. Their oocytes and corresponding embryos reveal compromised developmental competence due to multiple cellular defects, such as meiotic irregularities and mitochondrial dysfunction.[25] The old mouse model has been widely used in reproductive biology as an analogue to human female infertility due to advanced maternal age (≥35 years).[26]

Defective oocytes often contain compromised mitochondria, insufficient maternal endowment of proteins, and/or transcripts leading to chromosomal aneuploidy, particularly evident with aging.[25,27] Thus, it is anticipated that these molecular events may have impact on the cell membrane and cytoskeleton and therefore, lead to mechanical differences between defective and healthy oocytes. Cellular force-deformation measurements are expected to provide useful information for detecting oocyte dysfunctions.

All experiments were conducted in compliance with federal laws and institutional guidelines and were approved by the Mount Sinai Hospital Animal Care Committee in Toronto. Young and old ICR mice (Harlan Laboratories) were superovulated with 5IU of pregnant mare's serum gonadotropin (PMSG) (Sigma) and 48 h later with 5IU of human chorionic gonadotropin (hCG) (Sigma), by intraperitoneal injection. Mouse oocytes were collected from the superovluated female mice at 16 h post-hCG and cultured in potassium simplex optimization medium (KSOM, Specialty Media). The average diameter of the mouse oocytes was 96 μm.

Working principle of the cellular force measurement technique

Vision-based force measurement techniques are capable of retrieving both vision and force information from a single vision sensor (CCD/CMOS camera) under microscopy observation.[28,29] For cellular force measurement during cell manipulation, this concept is realized by visually tracking structural deformations of an elastic cell holding structure, and subsequently, transforming material deformations into forces.

The cell holding device shown in Fig. 1(b) integrates an array of cavities (180 μm in diameter) for accommodating individual mouse oocytes. Inside each cavity, low-stiffness micro-posts (45 μm high and 12 μm in diameter) are arranged in a circular pattern to support the oocyte during microinjection. Fig. 1(a) schematically illustrates the working principle of the cell holding device for vision-based cellular force measurement during oocyte injection. While the micropipette injects individual oocytes inside these cavities, applied forces are transmitted to the low-stiffness, supporting posts. In real time (30 Hz), a sub-pixel visual tracking algorithm measures post deflections that are fitted into an analytical mechanics model to calculate the force exerted on the oocyte.

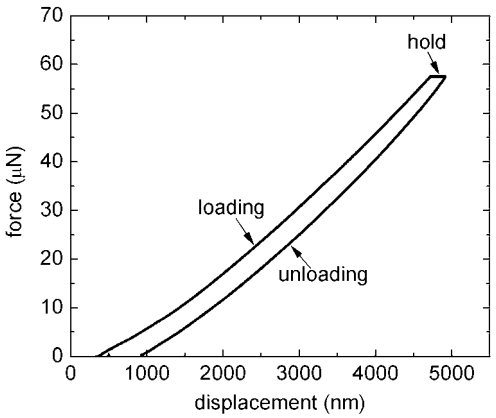

Fig. 2 A force-displacement curve of PDMS nanoindentation to calibrate the Young's modulus of cell holding devices.

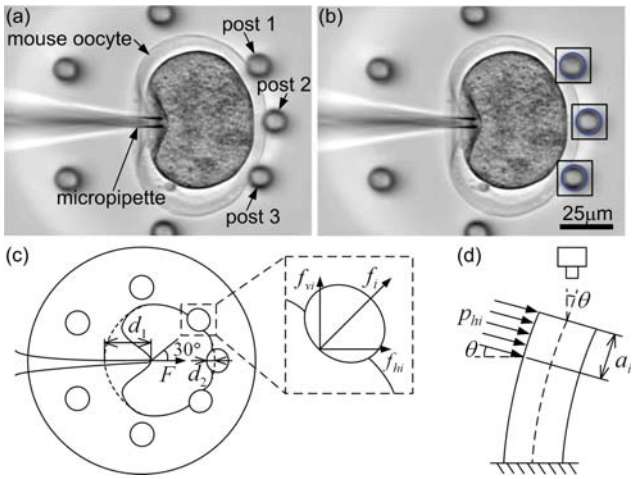

Fig. 3 (a) Indentation forces deform the mouse oocyte and deflect three supporting posts. (b) Image patches (black) tracked by template matching and LSCD detected post top circles (blue). (c) Force balance on the cell under indentation. (d) Post deflection model.

Device fabrication and characterization

The cell holding devices (Fig. 1(b)) were constructed with PDMS *via* standard soft lithography.[24] Briefly, PDMS prepolymer prepared by mixing Sylgard 184 (Dow Corning) and its curing agent with a weight ratio of 15 : 1, was poured over an SU-8 mold (SU-8 50, MicroChem) made on a silicon wafter using standard photolithography. After curing at 80 °C for 8 h, the PDMS devices were peeled off the SU-8 mold. The depth of the cavity and protruding posts is 45 μm, and the diameter of the posts is 12 μm (Fig. 1(b)). In order to make the PDMS surface hydrophilic, the devices were oxygen plasma treated for 10 s before use.

The mechanics model for mapping post deflections into cellular forces, discussed in the "Force Analysis" Subsection, requires the Young's modulus of the cell holding device to be accurately calibrated. Nanoindentation was used to determine the Young's modulus of the cell holding device and micro-posts. Five devices were calibrated using a nanoindentation instrument (TI-750 Ubi nanomechanical test instrument, Hysitron). Fig. 2 shows a calibration curve of applied forces *vs.* displacements. The determined Young's modulus value is 524.7 kPa ± 22.1 kPa (n = 5), which is within the range of previously reported values.[30]

Force analysis

Fig. 3(a) shows a snapshot captured in the cell injection process. A micromanipulator controls an injection micropipette to exert an indentation force to a mouse oocyte, deflecting the three supporting posts on the opposite side. Post deflections, measured by a visual tracking algorithm (discussed in "Visual Tracking of Post Deflections" Subsection) are fitted to an analytical mechanics model to obtain contact forces between the oocyte and posts. Based on the contact forces, the indentation force applied by the micropipette on the oocyte is determined through the following force analysis.

The oocyte is treated as elastic due to the fact that quick indentation by the micropipette does not leave sufficient time for cellular creep or relaxation to occur. The injection force, F is balanced by the horizontal components, f_{hi} of contact forces between the oocyte and supporting posts (Fig. 3(c)),

$$F = \sum_{i=1}^{3} f_{hi}, \quad i = 1,\ 2,\ 3 \tag{1}$$

In the device configuration, the radius of the oocyte (~48 μm) is larger than the depth of the cavity and posts (45 μm), resulting in an initial point contact between the oocyte and supporting posts before post deflections occur. However, the high deformability of mouse oocytes makes cell membrane conform to the posts when an injection force is applied to the oocyte. It is assumed that the contact forces are evenly distributed over the contact areas. Thus, the horizontal components, f_{hi} are expressed by a constant force intensity, p_{hi} and a contact length, a_i (Fig. 3(d))

$$f_{hi} = p_{hi} a_i, \quad i = 1,\ 2,\ 3 \tag{2}$$

Note that drag forces applied to the supporting posts by the fluidic environment were safely ignored, which were determined to be at a force level of 10^{-16} N using the fluidic drag model.[31]

Slope θ of the posts' free ends shown in Fig. 3(d) was measured to verify the validity of linear elasticity that requires small structural deflections. The maximum slope was determined to be 11.1°, which satisfies $\sin\theta \approx \theta$; thus, the small deflection assumption of linear elasticity holds.[32] Therefore, the relationship of the horizontal force intensity, p_{hi} and post deflections can be established.[32]

$$p_{hi} = \frac{\delta_i}{\dfrac{40a_i(1+\gamma)(2H-a_i)}{9\pi ED^2} + \dfrac{8\left(a_i^4 + 8H^3 a_i - 6H^2 a_i^2\right)}{3\pi ED^4}} \tag{3}$$

where $i = 1, 2, 3$; δ_i is the horizontal deflection; H and D are post height and diameter; E and γ are Young's modulus and Poisson's ratio ($\gamma = 0.5$ for PDMS[33]). In eqn (3), both bending and shearing of the supporting posts were considered since the post height/diameter ratio does not satisfy the pure bending assumption (height/diameter ratio > 5).[32]

Combining eqn (1)–(3) yields the injection force applied by the micropipette to the oocyte.

$$F = \sum_{i=1}^{3} \frac{\delta_i a_i}{\frac{40a_i(1+\gamma)(2H-a_i)}{9\pi ED^2} + \frac{8\left(a_i^4 + 8H^3 a_i - 6H^2 a_i^2\right)}{3\pi ED^4}} \quad (4)$$

In eqn (4), the unknown parameters are post horizontal deflections, δ_i and the contact length, a_i. Experimentally, imaging with a side-view microscope confirmed that the contact length, a_i increases at a constant speed, v_i for a given indentation speed. Hence, $a_i = v_i t$, where t denotes time.

Note that for a constant indentation speed of the micropipette, the variation speed of contact length a, v_i varies for different oocytes. At 60 μm/s used throughout the experiments, v_i of the tested mouse oocytes was measured to be 0.8 μm/s–1.2 μm/s. Interestingly, the sensitivity of the mechanics model (4) to variations in v_i is low. The injection force varies only by 1% when v_i changes from 0.8 μm/s to 1.2 μm/s. Thus, the average value of the measured speeds, 1 μm/s was used to calculate injection forces for all the oocytes.

Visual tracking of post deflections

In order to accurately track post deflections, a visual tracking algorithm with a resolution of 0.5 pixel was developed, which was described in detail previously.[24] A template matching algorithm tracks the motion of the supporting posts, providing processing areas for a least-squares circle detection (LSCD) algorithm to determine posts' center positions. The LSCD algorithm utilizes the Canny edge detector to obtain an edge image and then extracts a portion of the post top surface for circle fitting. The resolution of the visual tracking algorithm was determined by visually tracking the deflection of a stationary supporting post and calculating the standard deviation of the measured deflection data.

Electron microscopy imaging of zona pellucida (ZP)

ZP is a unique extracellular membrane (6–8 μm thick in mouse oocytes/embryos) surrounding the oocyte/embryo, which is composed of three types of glycoproteins arranged in a delicate filamentous matrix.[34] The ZP structure significantly contributes to the mechanical stiffness of the oocyte.[12,35] To understand the cause of possible subtle mechanical differences of healthy and defective oocytes, ZP surface morphology and glycoprotein structures were imaged using electron microscopy.

ZP surface morphologies of young and old oocytes were analyzed *via* scanning electron microscopy (SEM) imaging. Oocytes at 2 h post-collection were mounted on a Thermanox plastic coverslip (Fisher Scientific), fixed for 1 h with 2% glutaraldehyde in 1% sodium cacodylate buffer, postfixed for 1 h with 1% osmium tetroxide in 0.1 M sodium cacodylate buffer, and dehydrated in an acetone series of increasing concentration, according to a standard protocol.[36] After dehydration, the oocytes were CO_2 critical point dried in a polythene chamber, mounted on the specimen holder, coated with gold, and observed in an environmental SEM (XL-30, Philips).

Structural analysis of ZP glycoproteins was conducted *via* transmission electron microscopy (TEM) imaging of ZP cross-sections, following a standard method for sample preparation.[37] Young and old oocytes at 2 h post-collection were fixed for 1 h with 2% glutaraldehyde in 1% sodium cacodylate buffer, post-fixed for 1 h with 1% osmium tetroxide in 0.1 M sodium cacodylate buffer, embedded in agarose, cut into 100 nm thick sections, and observed in a TEM (CM-100, Philips).

F-actin staining

Oocyte mechanical properties are also regulated by the cytoskeleton. In this study, F-actin contents of the young and old ooyctes were quantified by fluorescence microscopy. F-actin of the oocytes were stained by fluorescein isothiocyanate (FITC) conjugated phalloidin. Oocytes at 2 h post-collection were washed with phosphate buffered saline (PBS), fixed for 10 min with 4% formaldehyde in PBS, permeabilized with 0.1% Triton X-100 in PBS, and stained with a 5 μg/ml phalloidin-FITC solution in PBS for 60 min at room temperature. The concentration of 5 μg/ml and the staining time of 60 min were experimentally determined to guarantee the saturation of all F-actin binding sites for phalloidin-FITC.[38] Between consecutive steps, PBS washing was conducted three times. Nuclei of the oocytes were also stained with 4′-6-Diamidino-2-phenylindole (DAPI) for control purpose.

Finally, the stained oocytes were mounted with a 1 : 1 glycerol:PBS solution onto microscope slides, and analyzed on a deconvolution microscope (Olympus IX-70, Applied Precision Inc.) with a FITC filter. Ten 1 μm optical sections for each sample were obtained. Average fluorescent intensity of the ten optical sections was regarded as the F-actin content.

Statistical analysis

Experimental data were analyzed using student's t-test (SigmaStat 3.5, Systat Software Inc.). Plots with error bars represent means ± one standard deviation (s.d.).

Results

All the experiments were conducted at 37 °C inside a temperature-controlled chamber. With a 40× objective (NA 0.55), the pixel size of the imaging system was calibrated to be 0.24 μm × 0.24 μm. Micropipette tips used for indenting mouse oocytes were 5.3 μm in diameter.

The template matching algorithm and the LSCD algorithm together cost 22.3 ms for processing each frame of image. Fig. 3(b) shows the tracked image patches and LSCD detected post top circles. The tracking resolution was determined to be 0.5 pixel (*i.e.*, 0.12 μm).

Force-deformation measurement and mechanical characterization results

A transfer pipette was used to deliver 20 young oocytes and 20 old oocytes onto the cell holding devices. The micropipette was controlled to indent each oocyte by 25 μm at 60 μm/s. During the indentation process, force data were collected (30 data points per second). Fig. 4(a) shows force-deformation curves of both young and old oocytes. The horizontal axis represents cell deformation, $d = d_1 + d_2$, where d_1 and d_2 were defined in Fig. 3(c). The d values were calculated by subtracting the deflections of post 2 (Fig. 4(a)) from the displacements of the

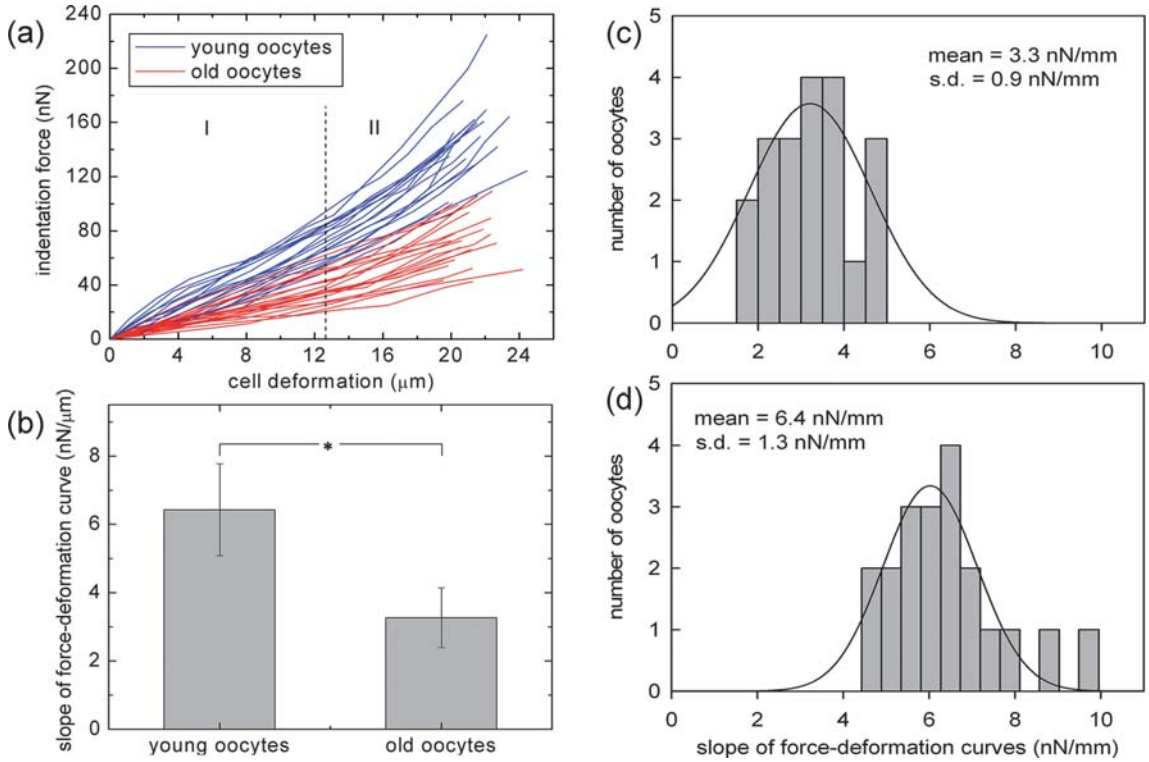

Fig. 4 (a) Force-deformation curves of young (blue) and old (red) oocytes. (b) Means ± one standard deviations of force-deformation curve slopes from young and old oocytes (* $p < 0.001$). (c)(d) Distribution histogram of the slopes of the force-deformation curves from (c) young oocytes and (d) old oocytes. There is a small overlap (4.4 nN/μm–4.8 nN/μm) of slopes between young and old oocytes.

injection micropipette. The vertical axis is the cellular force. Force measurement resolution of the system is defined as the finest force that a supporting post can measure, which is equal to the product of the stiffness of a suspended supporting post (16.8 nN/μm for current devices) and the tracking resolution of the post deflections (0.12 μm). The force measurement resolution was determined to be 2 nN at 30 Hz.

Most of the force-deformation curves of young and old oocytes separate themselves into two distinct areas with a slight overlap of a few curves. It was also observed that during microinjection, only ZP was deformed with cell deformation less than a certain value (12.7 μm ± 3.4 μm, n = 40; no significant difference (P = 0.487) between young and old oocytes), corresponding to region I in Fig. 4(a) where ZP stiffness is dominant. After the cell deformation was beyond 12.7 μm ± 3.4 μm (region II in Fig. 4(a)), both ZP and cytoplasm were deformed. Thus, the force-deformation data in region II reflect the overall stiffness of the ZP and cytoplasm.

Slopes of the force-deformation curves were calculated using linear regression, which is considered as oocytes' overall stiffness. Fig. 4(b) shows the means ± s.d. of the slopes of young and old oocytes. It was found that old oocytes have significantly lower stiffness ($p < 0.001$) than young oocytes (young oocytes: 6.4 ± 1.3 nN/μm, old oocytes: 3.3 ± 0.9 nN/μm). Fig. 4 (c)(d) illustrate the distribution histogram of the slopes of the force-deformation curves. There is a small overlap (4.4 nN/μm–4.8 nN/μm) of the slopes or stiffness values, with 10% (n = 20) of the young oocytes and 15% (n = 20) of the old oocytes falling into this overlapping region.

ZP structure analysis

In order to probe the cause of the detected mechanical changes in old oocytes, ZP thickness, surface morphology, and cross-sectional glycoprotein structures of young and old oocytes were analyzed by optical microscopy, SEM, and TEM imaging. Note that the measured stiffness of young and old oocytes was not correlated with the ZP structures of the same oocytes considering that indentation-induced global deformations of the ZP may change the ZP structures (*e.g.*, ZP thickness and glycoprotein density). ZP thickness of 16 young oocytes and 10 old oocytes was measured under an optical microscope (Nikon TE-2000S) with 400× magnification. For each oocyte, ZP thickness of five different locations was measured, and the average was taken as the final thickness value. The young oocytes have a ZP thickness of 7.1 μm ± 0.3 μm (mean±s.d.), which is not significantly different (p = 0.098) from that of young oocytes (6.8 μm ± 0.5 μm).

SEM imaging of ZP surfaces (Fig. 5) demonstrates that young and old oocytes reveal different surface morphologies. All observed young oocytes (n = 8) had a "spongy" surface comprised of multiple layers of networked glycoproteins with numerous pores (Fig. 5(a)), while only 20% of the old oocytes (n = 10) had similar surfaces. The other 80% of the old oocytes showed a rough surface without pores (Fig. 5(b)). The different ZP surface morphologies indicate different structures of ZP glycoproteins in young and old oocytes, which were then quantitatively analyzed *via* TEM imaging.

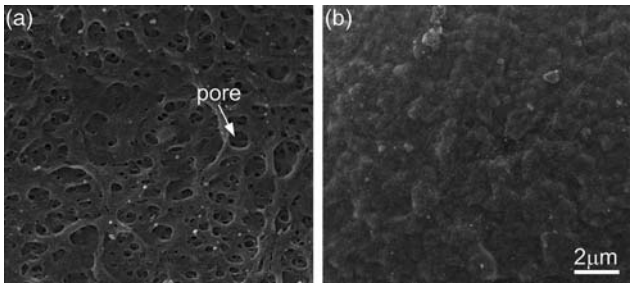

Fig. 5 Representative SEM images of ZP surfaces of (a) young and (b) old oocytes.

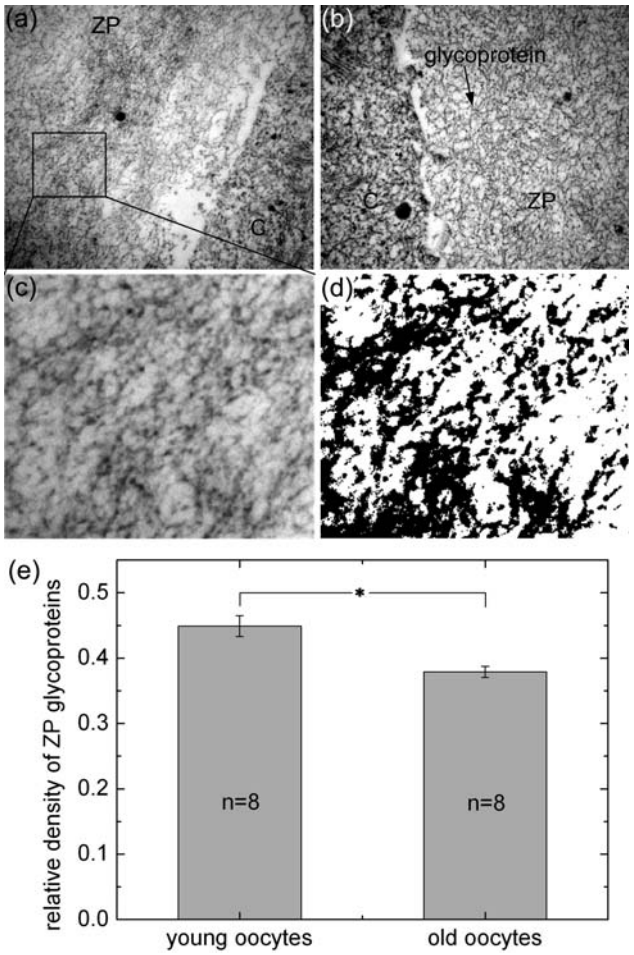

Fig. 6 (a)(b) Representative TEM images of cross sections of ZP glycoprotein structures from (a) young and (b) old oocytes (C: cytoplasm). (c) A sub-region from (a) for image processing. (d) Binary image after adaptive thresholding of (c). (e) Relative density of ZP glycoprotein structures of young and old oocytes (* $p < 0.001$).

Fig. 6(a)(b) show TEM cross-sectional views of the ZP glycoprotein structures from young (Fig. 6(a)) and old (Fig. 6(b)) oocytes. The density of ZP glycoproteins was quantified using image processing. An adaptive thresholding algorithm[7] was used to recognize the glycoprotein structure areas (black areas in Fig. 6(d)). The area ratio of glycoprotein structures to the total image is defined as the relative density of glycoproteins. The final relative density value of each oocyte was obtained from five different ZP regions by averaging. As shown in Fig. 6(e), the glycoproteins in old oocyte ZP are significantly sparser ($p < 0.001$) than those in young oocyte ZP. It is believed that the sparser ZP glycoproteins in old oocytes result in lower ZP stiffness than young oocytes, which mechanically differentiates young and old oocytes in region I of the force-deformation data (Fig. 4(a)).

F-actin contents

Fig. 7(a)(b) show F-actin staining of young and old oocytes, where the green and blue channels respectively represent F-actin and nucleus. Higher fluorescent intensity of the green channel indicates higher F-actin content. The fluorescence analysis results (Fig. 7(c)) show that old oocytes contain significantly less ($p < 0.001$) F-actin than young oocytes, which can be responsible for the stiffness difference in region II of the fore-deformation data (Fig. 4(a)). Contour line plots (Fig. 7(d)(e)) of F-actin fluorescence illustrate the F-actin distribution in the young and old oocytes. One can notice that the sub-cortical region of the old oocyte (labeled by white arrows in Fig. 7(e)) particularly lacks this cytoskeletal protein.

Discussion

Measurements of cell mechanical properties can be useful for predicting cellular response to mechanical stimuli and for

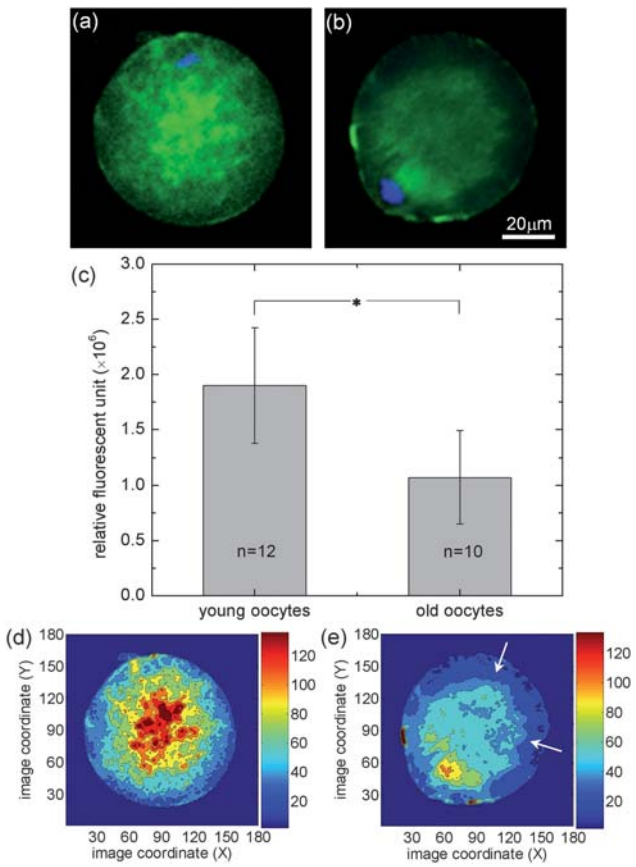

Fig. 7 F-actin content analysis. (a)(b) F-actin staining images of (a) young and (b) old oocytes. Green: F-actin. Blue: nucleus. (c) F-actin contents of young and old oocytes (* $p < 0.001$). (d) Contour line plot of F-actin fluorescence in (a). (e) Contour line plot of F-actin fluorescence in (b).

correlating mechanical properties to disease states.[4,39] Characterizing mammalian oocytes during microinjection without a separate characterization process promises a useful and low-cost approach to measure cellular mechanical properties. In this study, a vision-based cellular force measurement technique was developed to resolve nanonewton-level cellular forces and characterize oocyte stiffness. Young and aged mouse ooyctes were used as a comparison model. The technique can also be applied to characterize mechanical properties of mouse embryos by indenting those embryos using a micropipette without penetration. The experimental results demonstrated that the technique could be useful to detect potential oocyte defects and select high-quality oocytes for subsequent *in vitro* fertilization (IVF) and implantation.

The assessment of the reproductive quality of oocytes for IVF applications is an important procedure in assisted reproduction technologies (ART). The state-of-the-art morphology analysis method[40,41] is often subjective and fails to provide definitive prediction for oocyte quality, causing low pregnancy rates and therefore, imposing extra difficulties on the follow-up reproductive studies. Emerging techniques for oocyte quality assessment, such as genetic screening,[42,43] spectroscopy-based metabolomic profiling,[44–46] and polscope-based spindle imaging,[47,48] have following limitions: (1) the invasive deoxyribonucleic acid (DNA) sampling procedure that may impair the oocytes and result in lower development competence;[49] or (2) the requirement of specific analysis equipment[44–48] and complex spectral data analysis.[44–46]

The cellular force measurement technique can possibly provide a useful cue for oocyte quality assessment during microinjection. Experimental results proved the effectiveness of the technique for resolving subtle mechanical changes of old oocytes, due to structural changes of the ZP and cytoskeleton. These cellular structure changes are speculated to result from the aging-induced defects of old oocytes. F-actin structures were analyzed in the experiments; however, structures of other cytoskeletal filaments (*e.g.*, intermediate filament and microtubule) may also contribute to the measured mechanical differences between young and old mouse oocytes, which could spark further studies of cytoskeletal structure changes in old oocytes.

Previous studies have demonstrated that all ZP glycoprotein genes (ZP1, ZP2, and ZP3) downregulate in oocytes of old C57BL/6 mice,[25] which may explain the lower glycoprotein density of old oocytes observed in our experiments. In addition, cytoskeleton-related genes, such as Krt8 and Myo10 also have a lower expression in the old C57BL/6 mouse oocytes.[25] Krt8 is a member of the type II keratin gene family, and its protein product forms intermediate filaments of the cytoskeleton. Myo10 is a gene for encoding Myosin-X, which is a motor protein involved in cell motility. Reproductive biologists are still trying to uncover downregulated genes in old oocytes responsible for F-actin expression, which would interpret the low F-actin contents in old oocytes. Further studies are required to more clearly decipher the regulation pathways of these downregulated genes in mouse ooyctes to better understand the connection of ooycte defects and ZP/cytoskeleton structure changes.

Possible insignificant error sources of the cellular force measurement in this study include: (1) the assumption that the contact forces between the cell and supporting posts are evenly distributed over the contact areas; (2) the use of an average value of v_i, which can induce a force measurement error of $\leq$1%; (3) the Young's modulus calibration uncertainty (4.2%) of the PDMS cell holding devices; and (4) the visual tracking error for post deflection measurements ($\leq$0.5 pixel). Taking into account all the countable error sources (2)–(4), the measurement error of cellular forces was calculated to be $\leq$6.3%.

The cellular force measurement platform is not scale dependent. Different from mouse oocytes, the majority of suspended cells have a smaller size. The present PDMS cell holding devices can be scaled down to accommodate cells of smaller sizes. Soft lithography permits the construction of PDMS structures with an aspect ratio up to 10 : 1 (post height *vs.* post diameter) *via* process optimization. For example, a cell holding device with supporting posts of 10 μm in height and 2 μm in diameter (aspect ratio: 5 : 1; mechanical stiffness of each post: 1.2 nN/μm), based on a 0.5 pixel visual tracking resolution obtained in this study, has the capability of visually resolving forces down to 145 pN with a 40× objective. Thus, the device design and visual tracking algorithm provide a cost-effective, useful experimental platform for single cell studies with a sub-nanonewton force measurement resolution.

Conclusion

This paper demonstrated a vision-based cellular force measurement technique and its application to *in situ* mechanical characterization of mouse oocytes. By visually tracking deflections of elastic, low-stiffness supporting posts on a PDMS cell holding device during microinjection, the technique measured cellular forces in real time (30 Hz) with a 2 nN resolution. An analytical mechanics model was developed to convert post deflections into cellular forces. Young's modulus of the cell holding devices was calibrated to be 524.7 kPa $\pm$ 22.1 kPa (n = 5). Based on characterization experiments of 20 young mouse oocytes and 20 old mouse oocytes, it was found that the *in situ* obtained force-deformation data are useful for distinguishing healthy oocytes from defective ones. The follow-up analysis of oocyte structures also demonstrated that the subtle mechanical differences between young and old mouse oocytes may be due to structure changes of the zona pellucida and cytoskeleton.

Acknowledgements

We thank Douglas Holmyard for the assistance with SEM/TEM sample preparation, Zahra Mirzaei for assistance with F-actin staining, Richard Nay from Hysitron for use of nanoindentation equipment, and the staff in microfabrication center at the Emerging Communications Technology Institute (ECTI) of University of Toronto. This work was supported by the Natural Sciences and Engineering Research Council of Canada, the Ontario Ministry of Research and Innovation, and the Ontario Centers of Excellence. We also acknowledge the financial support from the Canada Research Chairs program to YS and the Ontario Graduate Scholarship program to XYL.

References

1 D. H. Kim, P. K. Wong, J. Park, A. Levchenko and Y. Sun, *Annu. Rev. Biomed. Eng.*, 2009, **11**, 203–233.
2 S. Suresh, *Acta Biomater.*, 2007, **3**, 413–438.

3 P. A. Janmey and C. A. McCulloch, *Annu. Rev. Biomed. Eng.*, 2007, **9**, 1–34.
4 G. Y. Lee and C. T. Lim, *Trends Biotechnol.*, 2007, **25**, 111–118.
5 C. A. Simmons, *J. Am. Coll. Cardiol.*, 2009, **53**, 1456–1458.
6 R. M. Hochmuth, *J. Biomech.*, 2000, **33**, 15–22.
7 X. Y. Liu, Y. F. Wang and Y. Sun, *IEEE Trans. Autom. Sci. Eng.*, 2009, **6**, 536–543.
8 J. W. Dai and M. P. Sheetz, *Biophys. J.*, 1995, **68**, 988–996.
9 J. Guck, R. Ananthakrishnan, H. Mahmood, T. J. Moon, C. C. Cunningham and J. Kas, *Biophys. J.*, 2001, **81**, 767–784.
10 G. T. Charras, P. P. Lehenkari and M. A. Horton, *Ultramicroscopy*, 2001, **86**, 85–95.
11 A. R. Bausch, F. Ziemann, A. A. Boulbitch, K. Jacobson and E. Sackmann, *Biophys. J.*, 1998, **75**, 2038–2049.
12 Y. Sun, K. T. Wan, K. P. Roberts, J. C. Bischof and B. J. Nelson, *IEEE Trans. NanoBiosci.*, 2003, **2**, 279–286.
13 S. Yang and T. Saif, *Exp. Cell Res.*, 2005, **305**, 42–50.
14 A. K. Harris, P. Wild and D. Stopak, *Science*, 1980, **208**, 177–179.
15 K. A. Beningo and Y. L. Wang, *Trends Cell Biol.*, 2002, **12**, 79–84.
16 J. L. Tan, J. Tien, D. M. Pirone, D. S. Gray, K. Bhadriraju and C. S. Chen, *Proc. Natl. Acad. Sci. U. S. A.*, 2003, **100**, 1484–1489.
17 O. du Roure, A. Saez, A. Buguin, R. H. Austin, P. Chavrier, P. Siberzan and B. Ladoux, *Proc. Natl. Acad. Sci. U. S. A.*, 2005, **102**, 2390–2395.
18 Y. Zhao and X. Zhang, *Sens. Actuators, A*, 2006, **125**, 398–404.
19 Y. N. Xia and G. M. Whitesides, *Angew. Chem., Int. Ed.*, 1998, **37**, 550–575.
20 N. J. Sniadecki, A. Anguelouch, M. T. Yang, C. M. Lamb, Z. Liu, S. B. Kirschner, Y. Liu, D. H. Reich and C. S. Chen, *Proc. Natl. Acad. Sci. U. S. A.*, 2007, **104**, 14553–14558.
21 W. Wang, X. Liu, D. Gelinas, B. Ciruna and Y. Sun, *PLoS One*, 2007, **2**, e862.
22 Y. Kimura and R. Yanagimachi, *Biol. Reprod.*, 1995, **52**, 709–720.
23 X. Y. Liu and Y. Sun, in *IEEE Int. Conf. on Robotics and Automation*, Kobe, Japan, 2009, pp. 526–531.
24 X. Y. Liu, Y. Sun, W. H. Wang and B. M. Lansdorp, *J. Micromech. Microeng.*, 2007, **17**, 1281–1288.
25 T. Hamatani, G. Falco, H. Akutsu, C. A. Stagg, A. A. Sharov, D. B. Dudekula, V. VanBuren and M. S. H. Ko, *Hum. Mol. Genet.*, 2004, **13**, 2263–2278.
26 G. I. Perez, A. Jurisicova, T. Matikainen, T. Moriyama, M. R. Kim, Y. Takai, J. K. Pru, R. N. Kolesnick and J. L. Tilly, *FASEB J*, 2005, **19**, 860–862.
27 N. M. Steuerwald, M. G. Bermudez, D. Wells, S. Munne and J. Cohen, *Reproductive BioMedicine Online*, 2007, **14**, 700–708.
28 Y. H. Luo and B. J. Nelson, *Journal of Robotic Systems*, 2001, **18**, 103–117.
29 M. A. Greminger and B. J. Nelson, *IEEE Trans. Pattern Anal. Mach. Intell.*, 2004, **26**, 290–298.
30 D. Armani, C. Liu and N. Aluru, in *IEEE International Conference on Micro Electro Mechanical Systems*, Orlando, FL, USA, 1999, pp. 222–227.
31 W. F. Hughes and J. A. Brighton, *Schaum's outline of theory and problems of fluid dynamics*, McGraw Hill, New York, 1999.
32 A. C. Ugural and S. K. Fenster, *Advanced strength and applied elasticity*, Prentice Hall PTR, Upper Saddle River, N.J., 2003.
33 J. E. Mark, *Polymer data handbook*, Oxford University Press, Oxford; New York, 2009.
34 G. Familiari, M. Relucenti, R. Heyn, G. Micara and S. Correr, *Microsc. Res. Tech.*, 2006, **69**, 415–426.
35 Y. Murayama, J. Mizuno, H. Kamakura, Y. Fueta, H. Nakamura, K. Akaishi, K. Anzai, A. Watanabe, H. Inui and S. Omata, *Hum. Cell*, 2006, **19**, 119–125.
36 C. Nogués, M. Ponsa, F. Vidal, M. Boada and J. Egozcue, *Journal of In Vitro Fertilization and Embryo Transfer*, 1988, **5**, 225–229.
37 Y. Martinova, M. Petrov, M. Mollova, P. Rashev and M. Ivanova, *Anim. Reprod. Sci.*, 2008, **108**, 425–434.
38 J. Bereiter-Hahn and J. Kajstura, *Histochemistry*, 1988, **90**, 271–276.
39 C. S. Chen, M. Mrksich, S. Huang, G. M. Whitesides and D. E. Ingber, *Science*, 1997, **276**, 1425–1428.
40 L. Scott, A. Finn, T. O'Leary, S. McLellan and J. Hill, *Hum. Reprod.*, 2007, **22**, 230–240.
41 L. Rienzi, F. Ubaldi, M. Iacobelli, S. Romano, M. G. Minasi, S. Ferrero, F. Sapienza, E. Baroni and E. Greco, *Reproductive BioMedicine Online*, 2005, **10**, 669–681.
42 P. Donoso, C. Staessen, B. C. J. M. Fauser and P. Devroey, *Hum. Reprod. Update*, 2007, **13**, 15–25.
43 G. Sher, L. Keskintepe, M. Keskintepe, M. Ginsburg, G. Maassarani, T. Yakut, V. Baltaci, D. Kotze and E. Unsal, *Fertil. Steril.*, 2007, **87**, 1033–1040.
44 R. Scott, E. Seli, K. Miller, D. Sakkas, K. Scott and D. H. Burns, *Fertil. Steril.*, 2008, **90**, 77–83.
45 C. G. Vergouw, L. L. Botros, P. Roos, J. W. Lens, R. Schats, P. G. A. Hompes, D. H. Burns and C. B. Lambalk, *Hum. Reprod.*, 2008, **23**, 1499–1504.
46 Z. P. Nagy, S. Jones-Colon, P. Roos, L. Botros, E. Greco, J. Dasig and B. Behr, *Reproductive BioMedicine Online*, 2009, **18**, 219–225.
47 J. H. Moon, C. S. Hyun, S. W. Lee, W. Y. Son, S. H. Yoon and J. H. Lim, *Hum. Reprod.*, 2003, **18**, 817–820.
48 L. Rienzi, F. Ubaldi, M. Iacobelli, M. G. Minasi, S. Romano and E. Greco, *Reproductive BioMedicine Online*, 2005, **10**, 192–198.
49 S. Mastenbroek, M. Twisk, J. van Echten-Arends, B. Sikkema-Raddatz, J. C. Korevaar, H. R. Verhoeve, N. E. Vogel, E. G. Arts, J. W. de Vries, P. M. Bossuyt, C. H. Buys, M. J. Heineman, S. Repping and F. van der Veen, *N. Engl. J. Med.*, 2007, **357**, 9–17.